Analysis and Design of Capacitive Power Transfer Systems Based on Induced Voltage Source Model

Shiying Wang, *Student Member, IEEE*, Junrui Liang, *Member, IEEE*, and Minfan Fu, *Senior Member, IEEE*

***Abstract*—Capacitive power transfer is a promising mid-range wireless charging technique. The existing induced current source model suffers from the coupling variation issue, which causes troubles in resonance design and compensation development. This article explores an induced voltage source model for the capacitive coupler. Using this model, the six coupling-dependent capacitors between each pair of plates are equivalently represented by the self-capacitors and induced voltage sources. The self-capacitance is verified to be coupling independent. Based on this model, the power transfer capability, the efficiency, and the influence of adding external shunt capacitors are easily analyzed. This model is very helpful in investigating the existing topology and developing new compensations, such as the CLL-L compensation. Finally, a capacitive coupler is built to verify the model, based on which a CLL-L compensation is implemented for constant output voltage application. The achieved system peak efficiency is 88%.**

***Index Terms*—Capacitive power transfer (CPT), induced voltage source (IVS) model, load-independent output voltage.**

I. Introduction

WIRELESS power transfer is an enabling technology to deliver power from the transmitter (TX) to the receiver (RX). It has shown great potentials in a variety of applications, such as the low-power sensors, portable devices, mobile phones, automatic pipeline, electric vehicles, and even high-speed trains [1]–[3]. Among all the potential solutions, the near-field inductive or capacitive coupling method is attractive because of its high efficiency for mid-distance power transfer [4], [5]. In the last decades, the inductive power transfer (IPT) has drawn dramatic attentions from both industrial and academic sectors [6], [7]. However, the demerit of the IPT comes from its sensitivity to surrounding conductive object, which may be heated by the induced eddy current in the magnetic field [8]–[10]. As duality of IPT, the capacitive power transfer (CPT), which utilizes the electric field coupling, is becoming a promising alternative solution for wireless charging. Compared to IPT, CPT has several attractive and unique benefits, such as low cost, no need of heavy magnetic cores, and no worry about the eddy-current loss in nearby metals [5], [11].

A CPT system usually needs two pairs of conductive plates, i.e., capacitive coupler, to have a complete ac current loop. From a circuit-point of view, the isolated coupler is usually modeled as lump capacitors [12]–[14]. In a resonance-based CPT system, the compensation topology and its resonant component parameters should be carefully designed to achieve the targets, such as specific power level, small voltage rating, and high efficiency [5], [11], [15]. In an IPT coupler, the coupling has clear physical meaning, i.e., the shared flux between TX and RX, which contributes to the power transfer. However, from a physical point of view, in a capacitive coupler, there are totally six mutual capacitors among four plates [16]. In most works, the couplers are purposely designed to avoid certain mutual coupling. For example, Huang *et al.* [10] used a coupler with long distance between TX plates, and then the coupler can be easily modeled as a series capacitor. Four mutual capacitances are considered in [17] while a pair of cross mutual capacitances are ignored. In order to build a compact system, the distance between each plate may not have such an amount of freedom for placement. In this scenario, all the mutual capacitances are comparable to each other, and it is not reasonable to ignore some of them. Therefore, it is of great importance to have a general and simple coupling model for the capacitive coupler, with which the circuit analysis and design can be dramatically simplified.

Several papers address the modeling issue for CPT coupler [16]–[18]. In [16], an induced current source (ICS) model is proposed to equivalently represent all the six mutual capacitors by a pair of shunt capacitors and ICSs. However, the shunt capacitances will change under position variation. If such kind of coupling-dependent capacitances are used for resonance, the achieved resonance frequency would naturally shift under coupling variation. In order to avoid this issue, the proposed compensations based on the ICS model have to use superposition law or complicated transfer equations to derive the required resonance conditions [16], [19]. It is interesting to find that the IPT system will not suffer from this issue because the inductive coupler is modeled by a pair of self inductors, which are naturally coupling-independent. Using the self-inductance for resonance, it is very straightforward to achieve load-independent output and zero-phase operation under a coupling-independent resonant frequency [20].

Manuscript received October 31, 2019; revised January 9, 2020; accepted March 9, 2020. Date of publication March 17, 2020; date of current version June 23, 2020. This work was supported in part by Shanghai Sailing Program under Grant 19YF1433700 and in part by Shanghai program for Professor of Special Appointment (Eastern Scholar, Youth). Recommended for publication by Associate Editor M. Vitelli. *(Corresponding author: Minfan Fu.)*

Shiying Wang is with ShanghaiTech University, Shanghai 201210, China; with Shanghai Advanced Research Institute, Chinese Academy of Sciences, Shanghai 201210, China, and also with the University of Chinese Academy of Sciences, Beijing 100049, China (e-mail: wangshy2@shanghaitech.edu.cn).

Junrui Liang and Minfan Fu are with ShanghaiTech University, Shanghai 201210, China (e-mail: liangjr@shanghaitech.edu.cn; fumf@shanghaitech.edu.cn).

Color versions of one or more of the figures in this article are available online at http://ieeexplore.ieee.org.

Digital Object Identifier 10.1109/TPEL.2020.2981675

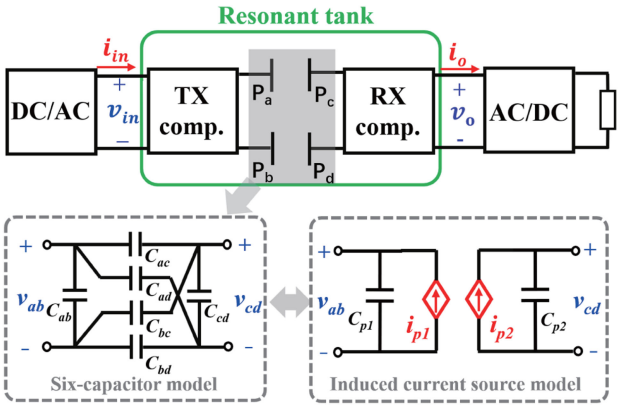

Fig. 1. CPT system configuration with the six-capacitor model and the ICS model of the capacitive coupler.

In order to simplify the CPT analysis and design, this article introduces the well-known induced voltage source (IVS) model for the capacitive coupler, based on which the success of IPT can be easily duplicated for CPT systems. Using this model, all the six mutual capacitances are represented through the series connection of a self-capacitance and an IVS for each side. Through analytical derivation and simulation, it shows that the self-capacitances of the IVS model are constant under various misalignment, but the ICS model could not meet this requirement. This attractive feature is exactly the same as that of the IPT coupler. Therefore, the well-developed IPT techniques can be directly introduced for the CPT counterpart. In this article, the power transfer capability, the coupler efficiency, and the effect of adding shunt capacitors are analytically discussed and explained. Meanwhile, the IVS model also significantly simplifies the compensation analysis and a novel CLL-L compensation is developed for applications with constant output voltage. Compared to the existing ICS model, the proposed IVS model is particularly promising for the coupler analysis, compensation design, and performance comparison.

II. Modeling of the Capacitive Coupler

A. Limitation of the ICS Model

A typical CPT system is shown in Fig. 1. The power is coupled from the TX plates (i.e., P_a and P_b) to the RX plates (i.e., P_c and P_d). Since the coupling is weak, both TX and RX compensations are necessary to boost the power transfer capability. This configuration is exactly the same as that of an IPT system. However, the capacitive coupling mechanism is much more complicated from a physical point of view. In a typical four-plate coupler, coupling exists between any two plates and there are usually six mutual capacitors [i.e., C_{ab}, C_{ac}, C_{ad}, C_{bc}, C_{bd}, and C_{cd} in Fig. 1]. Note that there is only one mutual inductor between two coupling coils in the counterpart IPT coupler. Therefore, it is significant to simplify the circuit model for the capacitive coupler. Here, v_{ab} and v_{cd} are the terminal voltage of the TX plates and RX plates, respectively. According to the equivalent circuit theory, any passive two-port network can be represented as two isolated parts with induced voltage/current source. In [16], the original six-capacitor model is represented by a pair of shunt capacitors and current sources (see Fig. 1) with the following equations:

$$\begin{cases} C_{p1} = C_{ab} + \frac{(C_{ac}+C_{ad})(C_{bc}+C_{bd})}{C_{ac}+C_{ad}+C_{bc}+C_{bd}} \\ C_{p2} = C_{cd} + \frac{(C_{ac}+C_{bc})(C_{ad}+C_{bd})}{C_{ac}+C_{ad}+C_{bc}+C_{bd}} \\ C_{pm} = \frac{C_{bd}C_{ac}-C_{ad}C_{bc}}{C_{ac}+C_{ad}+C_{bc}+C_{bd}} \\ k = \frac{C_{pm}}{\sqrt{C_{p1}C_{p2}}} . \end{cases} \tag{1}$$

In this model, C_{p1} and C_{p2} are the equivalent shunt capacitances; C_{pm} is the corresponding mutual capacitance; k is the coupling coefficient. The current source i_{p1} and i_{p2} are induced by the terminal voltage

$$\begin{cases} \boldsymbol{I_{p1}} = j\omega C_{pm}\boldsymbol{V_{cd}} \\ \boldsymbol{I_{p2}} = j\omega C_{pm}\boldsymbol{V_{ab}} . \end{cases} \tag{2}$$

Therefore, this model is named as the ICS model. In this article, I_{p1} and $\boldsymbol{I_{p1}}$ represent the magnitude and the phasor of i_{p1}. Similar rules are used to define all the other time-variant voltage or current, such as i_{p2} and v_{ab}.

Considering the popularity of the IVS model for IPT, it is very reasonable to accept the ICS model for CPT. This is mainly because of the circuit duality theory, such as inductors versus capacitors, or voltage source versus current source. Based on the well-developed IPT, the most appealing condition is that these mature IPT techniques can be directly introduced for its CPT counterpart. However, it is very difficult to derive the resonant frequency based on the ICS model, because the shunt capacitances (i.e., C_{p1} and C_{p2}) are coupling dependent. This phenomenon can be explained by the six-capacitor model. As shown in Fig. 1, the change of the relative position between the TX/RX plates (P_a, P_b, P_c, and P_d) leads to a varying mutual capacitance [i.e., C_{ab}, C_{ac}, C_{ad}, C_{bc}, C_{bd}, and C_{cd}], which would finally have coupling-dependent C_{p1} and C_{p2}. Under this condition, if C_{p1} or C_{p2} are designed for resonance, the resonance frequency will naturally shift under coupling variation. Therefore, the existing topologies using the ICS model have to use superposition law to analyze the resonance condition, and it is not very straightforward [5].

B. IVS Model

The IVS model is widely used for the IPT coupler due to its two unique benefits. First of all, the self-inductances in the IVS model are fixed and have clear physical meaning. Besides, all the coupling-dependent factors are represented by a pair of IVSs. Using this model, if the self-inductor is used for resonance, the achieved resonance frequency is naturally coupling independent. The IPT modeling experience actually can be directly introduced for the CPT by finding such fixed self-capacitances and coupling-dependent induced sources. Obviously, the ICS model does not meet this requirement.

In this article, the IVS model is proposed for the capacitive coupler, as shown in Fig. 2, where C_{tx} and C_{rx} are the self-capacitances of TX/RX plates; v_{tx} and v_{rx} are the equivalent IVS; i_{tx} and i_{rx} are the network input and output current, respectively.

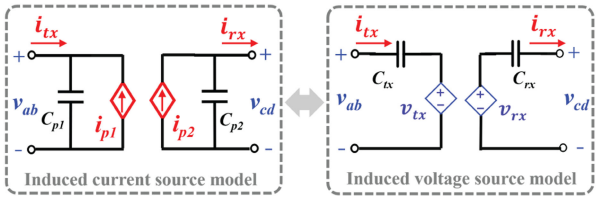

Fig. 2. Conversion between ICS model and IVS model.

For the ICS model, it has

$$\begin{bmatrix} \boldsymbol{I}_{\rm tx} \\ \boldsymbol{I}_{\rm rx} \end{bmatrix} = \begin{bmatrix} j\omega C_{p1} & -j\omega C_{pm} \\ j\omega C_{p2} & j\omega C_{pm} \end{bmatrix} \begin{bmatrix} \boldsymbol{V_{ab}} \\ \boldsymbol{V_{cd}} \end{bmatrix}. \tag{3}$$

Similarly, for the right-hand side IVS model, it has

$$\begin{bmatrix} \boldsymbol{V_{ab}} \\ \boldsymbol{V_{cd}} \end{bmatrix} = \begin{bmatrix} \frac{1}{j\omega C_{\rm tx}} & \frac{1}{j\omega C_m} \\ -\frac{1}{j\omega C_m} & \frac{1}{j\omega C_{\rm rx}} \end{bmatrix} \begin{bmatrix} \boldsymbol{I}_{\rm tx} \\ \boldsymbol{I}_{\rm rx} \end{bmatrix} \tag{4}$$

where C_m is the mutual capacitance in IVS model. Note C_m is different from C_{pm}. Combining (1), (3), and (4), it gives

$$\begin{cases} C_{\rm tx} = \frac{C_{p1}C_{p2} - C_{pm}C_{pm}}{C_{p2}} \\ C_{\rm rx} = \frac{C_{p1}C_{p2} - C_{pm}C_{pm}}{C_{p1}} \\ C_m = \frac{C_{p1}C_{p2} - C_{pm}C_{pm}}{C_{pm}}. \end{cases} \tag{5}$$

In this new model, the coupling coefficient k is defined as

$$k = \frac{\sqrt{C_{\rm tx}C_{\rm rx}}}{C_m} = \frac{C_{pm}}{\sqrt{C_{p1}C_{p2}}}. \tag{6}$$

It is interesting to find that this new-defined k is exactly the same as that of (1).

From a mathematical point of view, both $C_{\rm tx}$ and $C_{\rm rx}$ are derived based on C_{p1}, C_{p2}, and C_{pm}, which all look like to be coupling dependent. According to the ICS model in [16], C_{p1}, C_{p2}, and C_{pm} are all derived in terms of the six capacitors in (1). Taking this result into (5), $C_{\rm tx}$ and $C_{\rm rx}$ are derived in (7) and (8), shown at the bottom of this page. It is difficult to determine whether these capacitances are coupling dependent or not. Therefore, the self-capacitance should be analyzed from a circuit standpoint. Actually, $C_{\rm tx}$ is the input capacitance when $v_{\rm tx} = 0$, and this characteristic is exactly the same as that of the self-inductance in an IPT system. $v_{\rm tx} = 0$ can be achieved by opening the RX side (having $i_{\rm rx} = 0$) or removing the RX plates (having $k = 0$). It means the self-capacitance $C_{\rm tx}$ is only related to the area of P_a and P_b and the relative position between P_a and P_b, which are fixed for CPT applications. It should be noted that $C_{\rm tx}$ is not C_{ab} in Fig. 1. In the six-capacitor model, C_{ab} is a only part of overall equivalent capacitance between P_a and P_b. As shown in (7), only if the RX plates are removed, $C_{\rm tx} = C_{ab}$. In a real system, C_{ab} cannot be directly measured when RX plates exist, and its value is not fixed. However, $C_{\rm tx}$ is fixed and has clear physical meaning. This definition is exactly the same as that of an IPT system. Based on this modeling approach, most well-developed IPT techniques can be directly introduced for CPT.

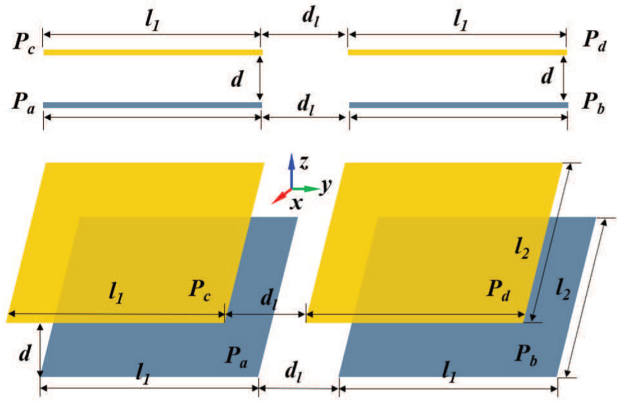

Fig. 3. Layout illustration of capacitive coupler.

C. Simulation Verification

A simulation is built in Maxwell to verify the proposed model. Four identical square plates are used to form a capacitive coupler. Fig. 3 shows the structure and dimension of the plates. Plates P_a and P_c are placed face to face, so as for plate P_b and P_d. The plate dimension is $l_1 \times l_2 (= 300\ \text{mm} \times 300\ \text{mm})$, and the horizontal distance between the same-side plates is d_l $(= 180\ \text{mm})$. The simulated capacitive coupler is the same as that of [19]. In the simulation, it can directly measure the parameters of the six-capacitor model, and all the other capacitances used in ICS or IVS model are calculated based on (1), (7), and (8).

In the first case, the vertical distance between TX and RX d changes from 10 to 200 mm. The variation of the capacitances C_{ac}, C_{ab}, C_{ad} in the six-capacitor model are given in Fig. 4(a). Since the capacitive coupler is symmetric, only three capacitances in the six-capacitor model are shown in Fig. 4(a). In the simulation, these equivalent capacitors (i.e., C_{ac}, C_{ab}, and C_{ad}) are obtained by assigning 0-V voltage at plate P_b, P_c, and P_d and 1-V voltage at plate P_a. The absorbed charges at plate P_b, P_c, and P_d can reflect C_{ac}, C_{ab}, and C_{ad}. Since the charge absorption and distribution are closely related to the plate relative positions, all these internal capacitances are strongly coupling dependent.

The coupling coefficient k decreases with the increasing d, as shown in Fig. 4(b). Fig. 4(c) shows the capacitances in the ICS model are all dependent on the coupling. Unlikely, in the proposed IVS model, both $C_{\rm tx}$ and $C_{\rm rx}$ are fixed as shown in Fig. 4(d), and the only coupling-dependent capacitance is C_m.

$$C_{\rm tx} = C_{ab} + \frac{C_{ac}C_{ad}(C_{bc}+C_{bd}) + C_{bc}C_{bd}(C_{ac}+C_{ad}) + C_{cd}(C_{ac}+C_{ad})(C_{bc}+C_{bd})}{(C_{ac}+C_{bc})(C_{ad}+C_{bd}) + C_{cd}(C_{ac}+C_{ad}+C_{bc}+C_{bd})} \tag{7}$$

$$C_{\rm rx} = C_{cd} + \frac{C_{ad}C_{bc}(C_{ac}+C_{bd}) + C_{ac}C_{bd}(C_{ad}+C_{bc}) + C_{ab}(C_{ac}+C_{ad})(C_{bc}+C_{bd})}{(C_{ac}+C_{bc})(C_{ad}+C_{bd}) + C_{cd}(C_{ac}+C_{ad}+C_{bc}+C_{bd})} \tag{8}$$

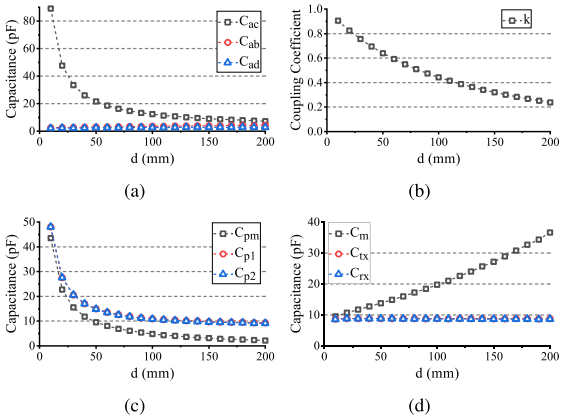

Fig. 4. Plates parameters at different d. (a) C_{ab}, C_{ad}, C_{ac} in the six-capacitor model. (b) Coupling coefficient k. (c) C_{p1}, C_{p2}, C_{pm} in the ICS model. (d) $C_{\rm tx}, C_{\rm rx}, C_m$ in the IVS model.

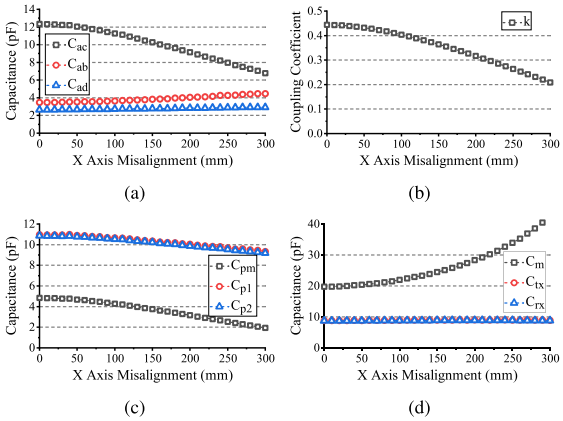

Fig. 5. Plates parameters under X-axis misalignment. (a) C_{ab}, C_{ad}, C_{ac} in the six-capacitor model. (b) Coupling coefficient k. (c) C_{p1}, C_{p2}, C_{pm} in the ICS model. (d) $C_{\rm tx}, C_{\rm rx}, C_m$ in the IVS model.

Besides the vertical distance variation, the misalignment conditions are also considered in this article. When d (= 100 mm) is fixed, the RX plates are moved along the X- and Y-axis, and the corresponding coupling variations are summarized in Figs. 5 and 6. The same conclusion can be drawn as Fig. 4. Therefore, the self-capacitances in the IVS model are coupling independent.

When RX side is removed, both C_{p1} and $C_{\rm tx}$ are the input capacitance of TX side. Thereby in Fig. 4, C_{p1} converges to $C_{\rm tx}$ with the increasing d. At the weak coupling region, C_{p1} becomes less sensitive to the coupling variation. Therefore, in terms of coupling dependence, the benefit of the IVS model is closely related to the application specifications (such as the coupler size, the transfer distance, and the misalignment tolerance). For strong coupling applications, like the charging of small devices, it is much more attractive to apply the IVS model.

III. Power Transfer Characteristics

A. Transfer Capability Improvement

In a practical CPT system, the power transfer capability needs to be boosted with proper compensation. As shown in Fig. 7,

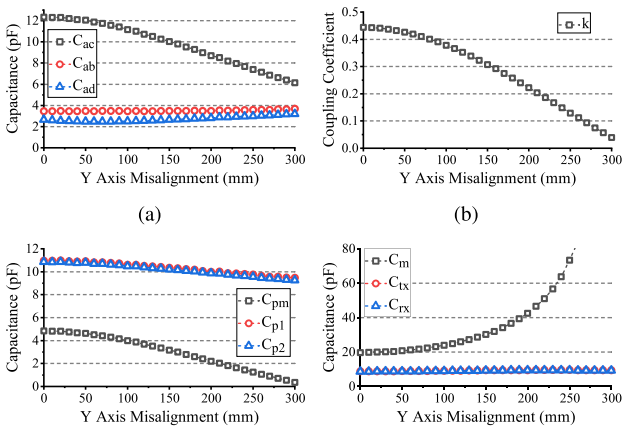

Fig. 6. Plates parameters under Y-axis misalignment. (a) C_{ab}, C_{ad}, C_{ac} in the six-capacitor model. (b) Coupling coefficient k. (c) C_{p1}, C_{p2}, C_{pm} in the ICS model. (d) $C_{\rm tx}, C_{\rm rx}, C_m$ in the IVS model.

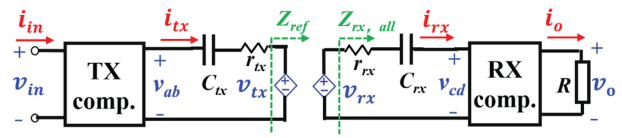

Fig. 7. CPT system using the induced voltage source model.

the TX and RX compensations are usually requested. Due to the duality between IPT and CPT, all the IPT compensations can find the counterpart in the CPT, such as the famous SS, SP, PS, PP, and LCC-C compensations [20], [21]. Since most of the compensation considerations of CPT are similar to those of IPT, only a brief discussion is given in the following.

In the IVS model, the power coupled from TX to RX is just the power aborted by $v_{\rm tx}$. Since the current passing through $v_{\rm tx}$ is $i_{\rm tx}$, the transferred real power is derived as

$$P_t = \text{real}[\boldsymbol{V}_{\rm tx}\boldsymbol{I}_{\rm tx}{}^*] = \frac{I_{\rm tx} I_{\rm rx} \sin\theta}{\omega C_m} \tag{9}$$

where * means the conjugate operation and θ is a phase difference between $i_{\rm tx}$ and $i_{\rm rx}$. When θ =90°, the power transfer is maximized. It means $v_{\rm rx}$ is in phase with $i_{\rm rx}$, and the equivalent impedance of RX side, i.e., $Z_{\rm rx,all}$, is purely resistive [refer to Fig. 7]. Meanwhile, this resistive $Z_{\rm rx,all}$ is reflected to the TX side as $Z_{\rm ref}$, which is also resistive and leads to zero phase between $v_{\rm tx}$ and $i_{\rm tx}$. θ is only affected by the RX compensation. The most straightforward compensation is to use a series inductor to resonate with $C_{\rm rx}$. At the TX side, the compensation is usually designed for zero-phase angle operation in order to reduce circulating energy.

B. Loss Analysis and Maximum Efficiency

In the previous study [5], [16], [19], the main loss of the CPT resonant tanks is caused by the coupling plates and the compensated inductors in series with $C_{\rm tx}$ and $C_{\rm rx}$. This article will concentrate on this part of losses, which are caused by the equivalent series resistor (ESR). As shown in Fig. 7, $r_{\rm tx}$ and $r_{\rm rx}$

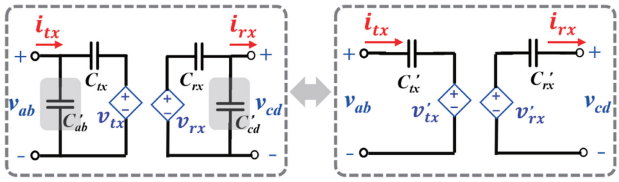

Fig. 8. IVS model with external shunt capacitors.

represent the overall ESRs of each side, respectively. Different to the inductive coupler, the losses due the compensation components are also significant. The quality factors are defined as

$$\begin{cases} Q_{\text{tx}} = 1/(\omega C_{\text{tx}} r_{\text{tx}}) \\ Q_{\text{rx}} = 1/(\omega C_{\text{rx}} r_{\text{rx}}). \end{cases} \tag{10}$$

For the resonant tank (i.e., from v_{in} to v_o), the overall loss is P_{loss}, which is slightly larger than the loss caused by r_{tx} and r_{rx}. It has

$$P_{\text{loss}} \geq {I_{\text{tx}}}^2 r_{\text{tx}} + {I_{\text{rx}}}^2 r_{\text{rx}} \geq 2 I_{\text{tx}} I_{\text{rx}} \sqrt{r_{\text{tx}} r_{\text{rx}}} = P_{\text{min}} \tag{11}$$

where P_{min} is the minimum loss.

When the power transfer capability is maximized, i.e., $\theta = 90°$. Taking (9) and (10) into (11) gives

$$P_{\text{min}} = 2\omega C_m P_t \sqrt{\frac{1}{Q_{\text{tx}} Q_{\text{rx}} \omega^2 C_{\text{tx}} C_{\text{rx}}}} = \frac{2P_t}{k\sqrt{Q_{\text{tx}} Q_{\text{rx}}}}. \tag{12}$$

Then, the efficiency of the resonant tank is

$$\eta \leq \eta_{\text{max}} = \frac{P_t}{P_{\text{min}} + P_t} = \frac{1}{1 + 2/(k\sqrt{Q_{\text{tx}} Q_{\text{rx}}})}. \tag{13}$$

η_{max} is the maximum efficiency of the resonant tank. It is only related to the quality factor and the coupling coefficient. Just like an IPT coupler, a high-Q CPT coupler can achieve high efficiency under strong coupling. Once a capacitive coupler is designed for a specific power level, the minimum power loss can be used to evaluate the efficiency before the real tests. P_{min} is achieved only if

$$P_{\text{min}} = {I_{\text{tx}}}^2 r_{\text{tx}} + {I_{\text{rx}}}^2 r_{\text{rx}} = 2 I_{\text{tx}} I_{\text{rx}} \sqrt{r_{\text{tx}} r_{\text{rx}}} \tag{14}$$

which further gives

$$I_{\text{tx}} \sqrt{r_{\text{tx}}} = I_{\text{rx}} \sqrt{r_{\text{rx}}}. \tag{15}$$

This condition equally means an optimal load is given at the RX side.

C. Influence of External Shunt Capacitors

In several papers [5], [19], external shunt capacitors are added, as shown in Fig. 8. These additional capacitors are helpful in reducing the required compensation inductance. However, its penalty is not mentioned. Based on the IVS model, the influence of these capacitors is better explained.

In Fig. 8, C'_{ab} and C'_{cd} are parallelly connected to the input and output terminal of the capacitive coupler. These capacitances can be viewed as a part of coupler, which means C'_{ab} and C'_{cd} are included in the six-capacitor model [refer to Fig. 1]. The Kirchhoff's current and voltage equations are given in (16), which is further represented by an IVS model in (17)

$$\begin{cases} \boldsymbol{I}_{\text{tx}} = \boldsymbol{I}_{\boldsymbol{C'_{ab}}} + \boldsymbol{I}_{\boldsymbol{C}_{\text{tx}}} = (\boldsymbol{V_{ab}} - \frac{\boldsymbol{I}_{\boldsymbol{C}_{\text{rx}}}}{j\omega C_m}) j\omega C_{\text{tx}} + j\omega C'_{ab} \boldsymbol{V_{ab}} \\ \boldsymbol{I}_{\text{rx}} = \boldsymbol{I}_{\boldsymbol{C'_{cd}}} + \boldsymbol{I}_{\boldsymbol{C}_{\text{rx}}} = (\boldsymbol{V_{cd}} - \frac{\boldsymbol{I}_{\boldsymbol{C}_{\text{tx}}}}{j\omega C_m}) j\omega C_{\text{rx}} + j\omega C'_{cd} \boldsymbol{V_{cd}} \\ \boldsymbol{V_{ab}} = \frac{\boldsymbol{I}_{\boldsymbol{C}_{\text{tx}}}}{j\omega C_{\text{tx}}} + \frac{\boldsymbol{I}_{\boldsymbol{C}_{\text{rx}}}}{j\omega C_m} \\ \boldsymbol{V_{cd}} = \frac{\boldsymbol{I}_{\boldsymbol{C}_{\text{rx}}}}{j\omega C_{\text{rx}}} + \frac{\boldsymbol{I}_{\boldsymbol{C}_{\text{tx}}}}{j\omega C_m} \\ k = \frac{\sqrt{C_{\text{tx}} C_{\text{rx}}}}{C_m}. \end{cases} \tag{16}$$

$$\begin{cases} C'_{\text{tx}} = C'_{ab} + \frac{(C'_{cd} + C_{\text{rx}}) C_{\text{tx}}}{C_{\text{rx}} + C'_{cd}(1-k^2)} \\ C'_{\text{rx}} = C'_{cd} + \frac{(C'_{ab} + C_{\text{tx}}) C_{\text{rx}}}{C_{\text{tx}} + C'_{ab}(1-k^2)} \\ C'_m = \frac{C_m (C'_{ab} + C_{\text{tx}})(C'_{cd} + C_{\text{rx}})}{C_{\text{tx}} C_{\text{rx}}} - \frac{C'_{ab} C'_{cd}}{C_m} \\ k' = \frac{\sqrt{C'_{\text{tx}} C'_{\text{rx}}}}{C'_m}. \end{cases} \tag{17}$$

When external capacitors are included, the modified IVS model [see (17) and Fig. 8] shows the increase of self-capacitance, which helps reduce the compensation inductance. However, this pair of new self-capacitances (C'_{tx} and C'_{rx}) are not fixed anymore under coupling variation, because both are affected by the real coupling coefficient k. This is a clear drawback by using additional capacitors.

The influence of these additional capacitors on the equivalent coupling coefficient k' is not very clear. The following discussion will show the external capacitors actually reduces the equivalent coupling. First of all, the square of the ratio between k'/k can be expressed as

$$\begin{aligned} \left(\frac{k'}{k}\right)^2 &= \left(\frac{\sqrt{C'_{\text{tx}} C'_{\text{rx}}}/C'_m}{\sqrt{C_{\text{tx}} C_{\text{rx}}}/C_m}\right)^2 \\ &= \frac{\alpha\beta}{(\alpha+\gamma)(\beta+\delta)} \end{aligned} \tag{18}$$

where $\alpha = C_m^2 C_{\text{tx}}$, $\beta = C_m^2 C_{\text{rx}}$, $\gamma = C_m^2 C'_{cd}(1-k^2)$, and $\delta = C_m^2 C'_{ab}(1-k^2)$. Since $\alpha, \beta, \gamma, \delta > 0$, it means $k'/k < 1$. Therefore, the new equivalent coupling coefficient becomes smaller. According to (13), a decreased coupling coefficient will lead to efficiency drop. Actually, a similar effect can be observed in an IPT system. Adding a series inductor with the self-inductor will reduce the equivalent coupling coefficient. However, an IPT system does not require additional series inductors because the self-inductances of the coupling coil are usually sufficiently large.

D. Uniform IVS Model

Due to the duality theory, both CPT and IPT can be described by a uniform IVS model as shown in Fig. 9. In this model, the self-impedances (Z_{tx} and Z_{rx}) are used instead of self-inductances or self-capacitances, and the mutual impedance Z_m is defined to replace the mutual inductance or capacitance. All the transfer characteristics are summarized in the following

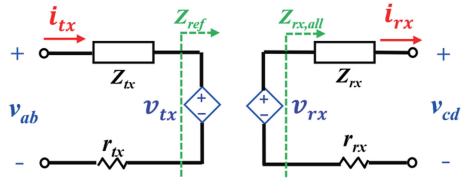

Fig. 9. Uniform IVS model for both CPT and IPT.

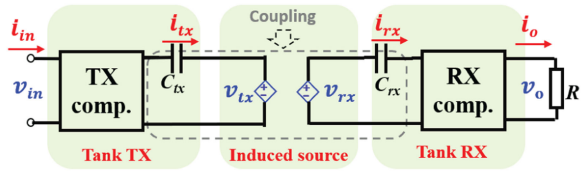

Fig. 10. System decomposition using the IVS model.

TABLE I
COMPARISON BETWEEN THE STUDY CASES

Compensation	LCLC [5]	LCL [16]	LC [22]
Frequency	1 MHz	1 MHz	1 MHz
Self capacitance	115 pF	380 pF	365 pF
Coupling coefficient	0.155	0.029	0.049
Quality factor	340	513	502
Output power: P_o	2400 W	1880 W	1074 W
Measured loss: P_{loss}	243 W	309 W	152 W
Estimated loss: P_{min}	91 W	246 W	87 W
Measured efficiency: η	90.8 %	85.9%	87.6%
Estimated efficiency: η_{max}	96.3%	88.4%	92.5%

equations:

$$\begin{cases} \boldsymbol{V}_{\rm tx} = \boldsymbol{Z_m} \boldsymbol{I}_{\rm rx} \\ \boldsymbol{V}_{\rm rx} = \boldsymbol{Z_m} \boldsymbol{I}_{\rm tx} \\ k = Z_m / \sqrt{Z_{\rm tx} Z_{\rm rx}} \\ \boldsymbol{Z}_{\rm ref} = {Z_m}^2 / \boldsymbol{Z}_{\rm rx,all} \\ Q_{\rm tx} = Z_{\rm tx} / r_{\rm tx} \\ Q_{\rm rx} = Z_{\rm rx} / r_{\rm rx} \\ P_t = Z_m I_{\rm tx} I_{\rm rx} \sin\theta \\ P_{\rm min} = 2P_t / (k\sqrt{Q_{\rm tx} Q_{\rm rx}}) \\ \eta_{\rm max} = 1/[1 + 2/(k\sqrt{Q_{\rm tx} Q_{\rm rx}})] \,. \end{cases} \tag{19}$$

This model is helpful to compare the coupler performance between CPT and IPT for a target application.

E. Comparison of Different CPT Couplers

In an IPT system, given the physical constraints (including the size, distance, and potential misalignment), the performance of the coupler can be easily compared based on the IVS model. For example, it is well known that the coupler efficiency will increase with the coil quality factor and the coupling coefficient, based on which it is able to determine which coupler is better and how to further improve the efficiency.

However, for the CPT systems reported in [5], [16], and [22], different couplers (different structure, size, and distance) are compensated with various networks. Even though the overall system efficiency is given, it is still difficult to understand the performance difference of the coupler. With the help of the IVS model, it is much more straightforward to address this issue. For all these CPT systems, both the quality factors and the coupling coefficients are derived in Table I. According to (19), the minimum losses $P_{\rm min}$ and the maximum efficiency $\eta_{\rm max}$ can both be estimated in Table I. This estimation well predicts the theoretically maximum efficiency. It clearly shows the low efficiency of [16] and [22] is mainly due to the small coupling coefficient. According to the conclusion of Section III-C, the small coupling coefficient in [22] is because of the additional shunt capacitors. In the future, it is particularly attractive to have a unique standard to evaluate inductive/capacitor couplers.

IV. RESONANCE ANALYSIS USING THE IVS MODEL

A. System Decomposition

The proposed IVS model can greatly simplify the circuit analysis, especially for high-order compensated CPT systems. The IVS model is used in [20] to develop the high-order IPT compensations. These systems enable the load-independent output and zero-phase operation under a resonant frequency, which will not shift under coupling variation. Similar accomplishments can be achieved in the CPT systems.

A high-order CPT system is decomposed as three parts in Fig. 10, including Tank TX, the induced source part, and Tank RX. $C_{\rm tx}$ and $C_{\rm rx}$ are in series with TX/RX compensations to form Tank TX/RX, respectively. The induced source part only includes $v_{\rm tx}$ and $v_{\rm rx}$. Since all the resonant components are fixed, the proposed decomposition method can naturally help to analyze all coupling-independent CPT topologies in a very simple and straightforward manner. Note that it will be much more complicated to use the coupling-dependent ICS model for the same objective, i.e., coupling-independent resonance.

B. Analysis of Existing Compensations

All the systems in [5], [16], and [19] are analyzed with ICS models, and complicated resonance condition is defined, which is difficult to understand the mechanism. Based on the IVS model, the resonance is much simpler to explain.

The double-sided *LCL* compensation serves as a study case in Fig. 11 [16]. The four coupling plates are placed vertically to ensure large C_{ab} and C_{cd} and there is no need to use external shunt capacitors. Once the IVS model is applied, the equivalent topology is given Fig. 11(b). This way, the new topology works like the double-sided LCC compensated IPT [6], and its resonance condition can be achieved by

$$\begin{cases} j\omega L_{f1} = -1/(j\omega C_{f1}) = j\omega L_1 - 1/(j\omega C_{\rm tx}) \\ j\omega L_{f2} = -1/(j\omega C_{f2}) = j\omega L_2 - 1/(j\omega C_{\rm rx}) \,. \end{cases} \tag{20}$$

Using Thevenin's and Norton's theory, the resonance mentioned above can ensure that $v_{\rm in}$ clamps $i_{\rm tx}$ (i.e., voltage source to current source, V2I) in the tank TX, $i_{\rm tx}$ induces $v_{\rm rx}$ (I2V) in

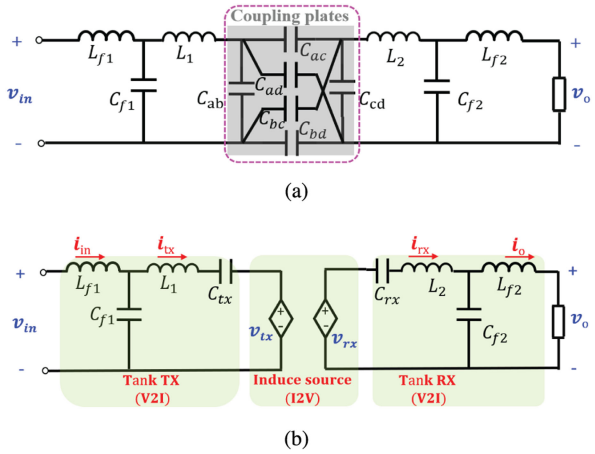

Fig. 11. Double-sided *LCL* compensation in [16]. (a) Original circuit model. (b) Equivalent circuit using the IVS model.

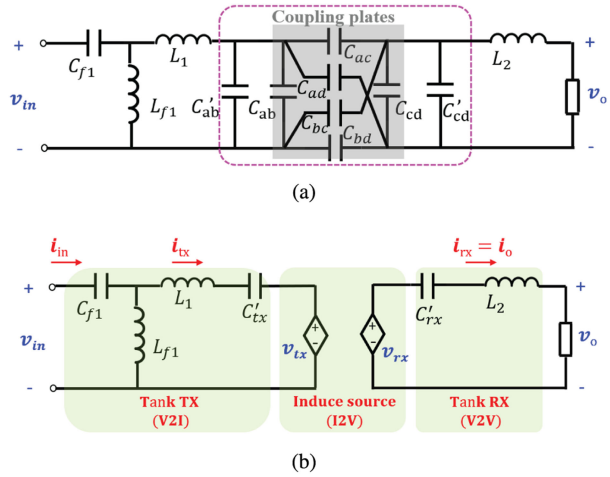

Fig. 12. Proposed CLL-L compensation for load-independent output voltage. (a) Original circuit model. (b) Equivalent circuit using the IVS model.

the induced source part, and $v_{\rm rx}$ controls i_o (V2I) in the tank RX. Finally, it can offer load-independent output current, i.e., i_o is linearly controlled by $v_{\rm in}$. The overall transfer function is

$$\frac{I_o}{V_{\rm in}} = \frac{\omega C_{f1} C_{f2}}{C_m} = \frac{\omega C_{f1} C_{f2}}{k\sqrt{C_{\rm tx} C_{\rm rx}}}. \tag{21}$$

The coupling will affect the gain, but will not affect the resonance frequency, because all the resonance components are coupling independent.

This example shows the benefits of the IVS model for the analysis of high-order compensated CPT systems. However, it also has its demerits compared to some general methods, such as the Gyrator model [23]. This model can derive all resonance frequencies for load-independent output. For example, when the leakage inductance or the mutual inductance (instead of the coupling-independent self-inductance) is properly used for resonance, the achieved resonance frequency can still offer load-independent output but the achieved frequency will shift under coupling variation. Therefore, different modeling approach does have its own merits when dealing with specific design objectives.

C. Development of New Compensation

The IVS model is helpful for the evaluation of exiting topology, and it also has a particular meaning for new topology development. Since the IPT compensation theory has been well developed in the past decades, based on a uniform IVS model, all the IPT compensations are able to find its duality in CPT applications. For example, the SS compensation in IPT is just the proposed double-sided *LC* compensation in [19]. Similarly, other widely used IPT compensations, such as SP, PS, PP, and LCC, can do the same thing. The rule is simple, replacing the inductor with the capacitor in a topology.

This article would serve as a start point for the CPT compensation theory. Here, a CLL-L compensation is proposed as an example, as shown in Fig. 12. A capacitive coupler with external capacitors are applied, and the IVS model is used to analyze the resonance. This CPT compensation is the duality of the LCC-C IPT compensation, which is famous for its load-independent

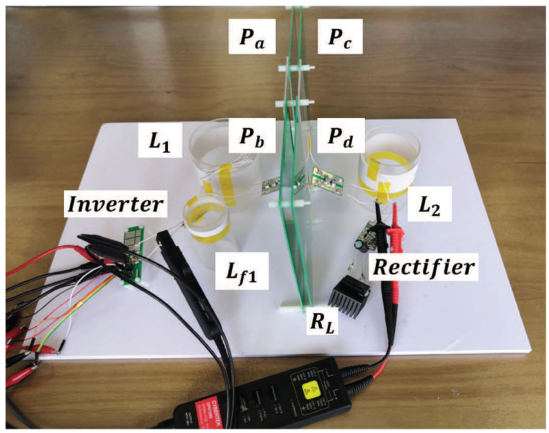

Fig. 13. CLL-L compensated CPT system.

output voltage ability. Therefore, the resonance condition can be easily explained and derived as

$$\begin{cases} j\omega L_{f1} = -1/(j\omega C_{f1}) = j\omega L_1 - 1/(j\omega C'_{\rm tx}) \\ j\omega L_2 = -1/(j\omega C'_{\rm rx})\,. \end{cases} \tag{22}$$

As shown in Fig. 12, the resonance of the first green block can make sure $i_{\rm tx}$ is controlled by $v_{\rm in}$, i.e., $\boldsymbol{I}_{\rm tx} = \boldsymbol{V}_{\rm in}/(j\omega L_{f1})$; The second green block ensures $\boldsymbol{V}_{\rm rx} = \boldsymbol{I}_{\rm tx} \boldsymbol{j\omega C_m}$; the series resonance within the third green block gives $\boldsymbol{V_o} = \boldsymbol{V}_{\rm rx}$. Finally, it has

$$\boldsymbol{V_o} = \frac{C_{f1}}{k'\sqrt{C'_{\rm tx} C'_{\rm rx}}} \boldsymbol{V}_{\rm in} = \frac{C_{f1}}{C_m} \boldsymbol{V}_{\rm in}. \tag{23}$$

V. Experimental Verification

A. Model Validation

A prototype CPT system is built, as shown in Fig. 13. The capacitive coupler is made of four printed circuit boards. In order to verify the proposed model, the self-capacitance $C_{\rm tx}$ in the IVS model and the shunt capacitance C_{p1} in the ICS model are measured by a network analyzer (N9915 A, Keysight Inc).

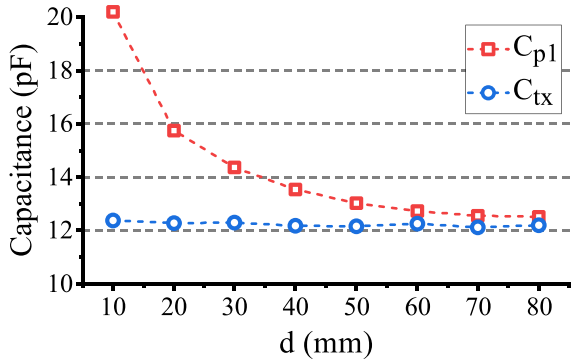

Fig. 14. Measured model parameters: C_{p1} in the ICS model and C_{tx} in the IVS model.

TABLE II
PARAMETERS OF THE PROPOSED CLL-L COMPENSATED CPT SYSTEM

Parameter	Design Value	Paramter	Design value
V_o/V_{in}	2	P_o	45W
l_1	120 mm	l_2	200 mm
d	10 mm	d_l	70 mm
C_{f1}	1715.7 pF	f_s	2 MHz
C_{tx}	12.58 pF	C_{rx}	12.58 pF
C'_{qb}	62.5 pF	C'_{cd}	125.1 pF
C'_m	857.9 pF	k'	0.12
C'_{tx}	76.6 pF	Q'_{tx}	343
C'_{rx}	138.3 pF	Q'_{tx}	449
L_{f1}	3.69 μ H	Q_{Lf1}	487
L_1	78.9 μ H	Q_{L1}	447
L_2	45.8 μ H	Q_{L2}	608

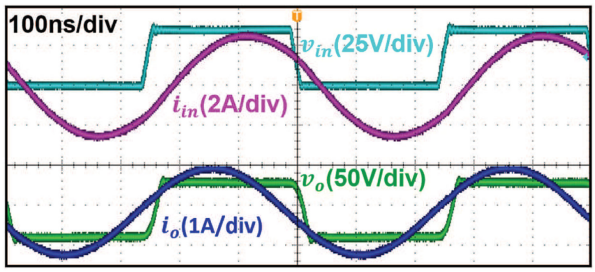

Fig. 15. Input and output waveforms.

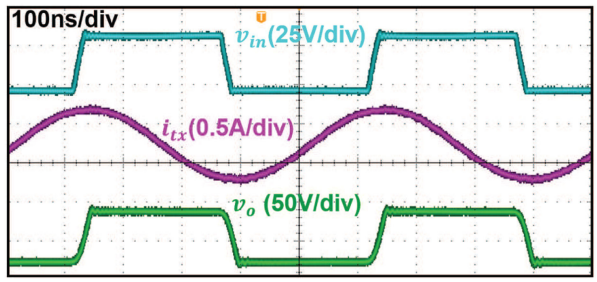

Fig. 16. Waveforms of v_{in}, i_{tx}, and v_o.

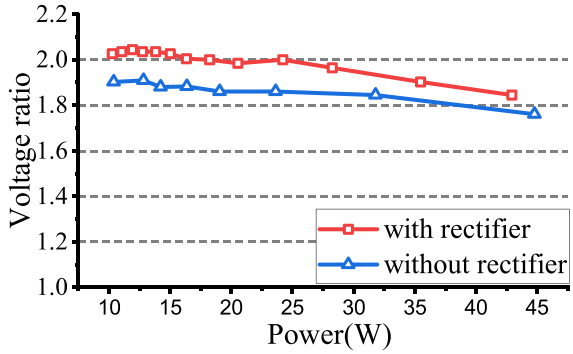

Fig. 17. Voltage ratio under different load condition when v_{in} is fixed.

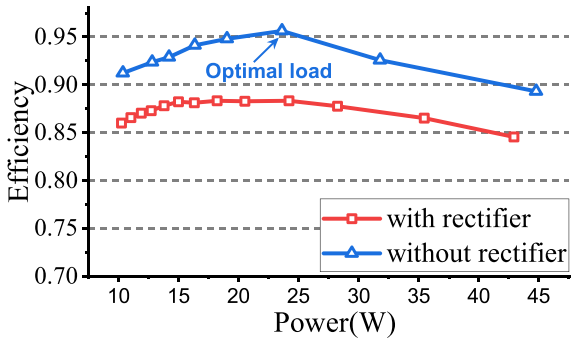

Fig. 18. Efficiency under different load condition when v_{in} is fixed.

Fig. 14 shows that C_{tx} is coupling independent, and C_{p1} gradually converges to C_{tx}.

B. CLL-L Compensation

Using the capacitive coupler, the proposed CLL-L compensation is implemented to verify the proposed resonance analysis method. All the system parameters are given in Table II. Since C_{tx} is very small, additional shunt capacitors are added. A half-bridge inverter and a full-bridge rectifier are used at input and output port. Both dc input and output are designed at 36 V. The resonant frequency is 2 MHz.

At full load condition, the experimental waveforms are measured, as shown in Fig. 15. The zero voltage switching is achieved by having a slightly inductive input impedance, which ensures v_{in} leading i_{in}. v_o slightly lags i_o due to the diode junction capacitance. The waveforms of v_{in}, i_{tx}, and v_o are given in Fig. 16, which shows v_{in} almost lags the i_{tx} by 90° and is in phase with v_o. All the phase relationships are consistent with the resonance's requirement (23).

When input voltage v_{in} is fixed, the voltage ratio is measured under different load conditions. Two different setups are tested, i.e., the system with rectifier and the one without rectifier. For both cases, the voltage ratio is compared in Fig. 17, and it shows that load-independent output voltage is realized.

The system efficiency is measured in Fig. 18, which shows that the peak dc–dc efficiency is 88% and the efficiency of the system without rectifier is 95%. This efficiency curve also shows the existence of an optimal loading point, which is consistent with the analysis in Section III-B. The maximum efficiency tracking is also valid for the CPT system [24]. Without the rectifier, the loss distribution is shown in Fig. 19 for full-load condition. In the proposed loss model, the ESRs of L_1 and L_2 are merged

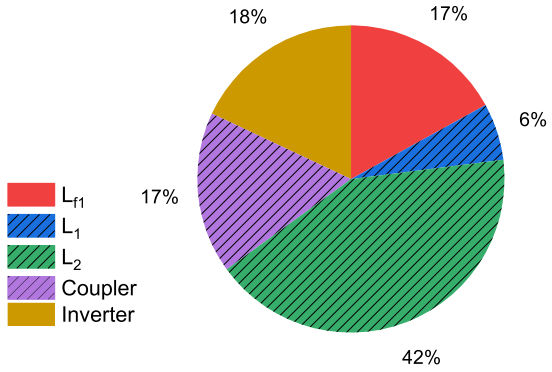

Fig. 19. Loss distribution.

into r_{tx} and r_{rx}, and the shade area (including the coupler, L_1 and L_2) serves well to evaluate the CPT efficiency.

VI. Conclusion

The IVS model for the CPT system is explored in this article. Using this model, the coupling-dependent capacitances are avoided and all the coupling-related factors are represented through a pair of IVSs. The accuracy of the modeling approach is justified by Maxwell simulation. This kind model approach is able to fully utilize the duality between IPT and CPT, and almost all the well-developed IPT techniques can be directly introduced for CPT. Based on an uniform impedance model for both IPT and CPT, the maximum efficiency and optimal load are easily derived for CPT. Besides, the model is also applied to analyze several existing compensations and their associated resonance mechanism. Finally, the IVS model is used to develop a new CPT compensation as the dual network for the famous LCC-C IPT compensation. The demonstrated CLL-L compensation can achieve load-independent output voltage with a peak efficiency at 88%.

References

[1] C.-H. Ou, H. Liang, and W. Zhuang, "Investigating wireless charging and mobility of electric vehicles on electricity market," *IEEE Trans. Ind. Electron.*, vol. 62, no. 5, pp. 3123–3133, May 2015.

[2] H. H. Wu, A. Gilchrist, K. D. Sealy, and D. Bronson, "A high efficiency 5 kW inductive charger for EVs using dual side control," *IEEE Trans. Ind. Inf.*, vol. 8, no. 3, pp. 585–595, Aug. 2012.

[3] J. Feng, Q. Li, F. C. Lee, and M. Fu, "Transmitter coils design for free-positioning omnidirectional wireless power transfer system," *IEEE Trans. Ind. Inf.*, vol. 15, no. 8, pp. 4656–4664, Aug. 2019.

[4] M. Fu, H. Yin, M. Liu, Y. Wang, and C. Ma, "A 6.78 MHz multiple-receiver wireless power transfer system with constant output voltage and optimum efficiency," *IEEE Trans. Power Electron.*, vol. 33, no. 6, pp. 5330–5340, Jun. 2018.

[5] F. Lu, H. Zhang, H. Hofmann, and C. Mi, "A double-sided LCLC-compensated capacitive power transfer system for electric vehicle charging," *IEEE Trans. Power Electron.*, vol. 30, no. 11, pp. 6011–6014, Nov. 2015.

[6] S. Li, W. Li, J. Deng, T. D. Nguyen, and C. C. Mi, "A double-sided LCC compensation network and its tuning method for wireless power transfer," *IEEE Trans. Veh. Technol.*, vol. 64, no. 6, pp. 2261–2273, Jun. 2015.

[7] M. Fu, H. Yin, and C. Ma, "Megahertz multiple-receiver wireless power transfer systems with power flow management and maximum efficiency point tracking," *IEEE Trans. Microw. Theory Techn.*, vol. 65, no. 11, pp. 4285–4293, Nov. 2017.

[8] Y.-G. Su, Y.-M. Zhao, A. P. Hu, Z.-H. Wang, C.-S. Tang, and Y. Sun, "An F-type compensated capacitive power transfer system allowing for sudden change of pickup," *IEEE J. Emerg. Sel. Topics Power Electron.*, vol. 7, no. 2, pp. 1084–1093, Jun. 2019.

[9] D. J. Graham, J. A. Neasham, and B. S. Sharif, "Investigation of methods for data communication and power delivery through metals," *IEEE Trans. Ind. Electron.*, vol. 58, no. 10, pp. 4972–4980, Oct. 2011.

[10] L. Huang, A. P. Hu, A. K. Swain, and Y. Su, "Z-impedance compensation for wireless power transfer based on electric field," *IEEE Trans. Power Electron.*, vol. 31, no. 11, pp. 7556–7563, Nov. 2016.

[11] C. Liu, A. P. Hu, B. Wang, and N.-K. C. Nair, "A capacitively coupled contactless matrix charging platform with soft switched transformer control," *IEEE Trans. Ind. Electron.*, vol. 60, no. 1, pp. 249–260, Jan. 2013.

[12] J. Dai and D. C. Ludois, "Single active switch power electronics for kilowatt scale capacitive power transfer," *IEEE J. Emerg. Sel. Topics Power Electron.*, vol. 3, no. 1, pp. 315–323, Mar. 2015.

[13] M. P. Theodoridis, "Effective capacitive power transfer," *IEEE Trans. Power Electron.*, vol. 27, no. 12, pp. 4906–4913, Dec. 2012.

[14] J. Dai and D. C. Ludois, "Capacitive power transfer through a conformal bumper for electric vehicle charging," *IEEE J. Emerg. Sel. Topics Power Electron.*, vol. 4, no. 3, pp. 1015–1025, Sep. 2016.

[15] J. Dai and D. C. Ludois, "A survey of wireless power transfer and a critical comparison of inductive and capacitive coupling for small gap applications," *IEEE Trans. Power Electron.*, vol. 30, no. 11, pp. 6017–6029, Nov. 2015.

[16] H. Zhang, F. Lu, H. Hofmann, W. Liu, and C. Mi, "A 4-plate compact capacitive coupler design and LCL-compensated topology for capacitive power transfer in electric vehicle charging applications," *IEEE Trans. Power Electron.*, vol. 31, no. 12, pp. 8541–8551, Dec. 2016.

[17] L. Huang and A. Hu, "Defining the mutual coupling of capacitive power transfer for wireless power transfer," *Electron. Lett.*, vol. 51, no. 22, pp. 1806–1807, Oct. 2015.

[18] C. Liu, A. P. Hu, and M. Budhia, "A generalized coupling model for Capacitive Power Transfer systems," in *Proc. 36th Annu. Conf. IEEE Ind. Electron. Soc.* Glendale, AZ, USA, Nov. 2010, pp. 274–279.

[19] F. Lu, H. Zhang, H. Hofmann, and C. C. Mi, "A double-sided LC-compensation circuit for loosely coupled capacitive power transfer," *IEEE Trans. Power Electron.*, vol. 33, no. 2, pp. 1633–1643, Feb. 2018.

[20] R. He, P. Zhao, M. Fu, Y. Liu, H. Wang, and J. Liang, "Decomposition and synthesis of high-order compensated inductive power transfer systems for improved output controllability," *IEEE Trans. Microw. Theory Techn.*, vol. 67, no. 11, pp. 4514–4523, Nov. 2019.

[21] Y. H. Sohn, B. H. Choi, E. S. Lee, G. C. Lim, G.-H. Cho, and C. T. Rim, "General unified analyses of two-capacitor inductive power transfer systems: Equivalence of current-source SS and SP compensations," *IEEE Trans. Power Electron.*, vol. 30, no. 11, pp. 6030–6045, Nov. 2015.

[22] H. Zhang, C. Zhu, and F. Lu, "Long-distance and high-power capacitive power transfer based on the double-sided LC compensation: Analysis and design," in *Proc. IEEE Transp. Electrific. Conf. Expo* Detroit, MI, USA, Jun. 2019, pp. 1–5.

[23] Y. H. Sohn, B. H. Choi, G. Cho, and C. T. Rim, "Gyrator-based analysis of resonant circuits in inductive power transfer systems," *IEEE Trans. Power Electron.*, vol. 31, no. 10, pp. 6824–6843, Oct. 2016.

[24] M. Fu, H. Yin, X. Zhu, and C. Ma, "Analysis and tracking of optimal load in wireless power transfer systems," *IEEE Trans. Power Electron.*, vol. 30, no. 7, pp. 3952–3963, Jul. 2015.

Shiying Wang (Student Member, IEEE) received the B.S degree in electrical engineering and automation from Guangzhou University, Guangzhou, China, in June, 2017. She is currently working toward the M.S. degree with the School of Information Science and Technology, ShanghaiTech University, Shanghai, China.

Her research interests include modeling and compensation networks of CPT systems.

Junrui Liang (Member, IEEE) received the B.E. and M.E. degrees in instrumentation engineering from Shanghai Jiao Tong University, Shanghai, China, in 2004 and 2007, respectively, and the Ph.D. degree in mechanical and automation engineering from The Chinese University Hong Kong, Hong Kong, in 2010.

He has been an Assistant Professor with the School of Information Science and Technology, ShanghaiTech University, Shanghai, China, since 2013. His research interests include energy conversion and power conditioning circuits, kinetic energy harvesting and vibration suppression, mechatronics, and IoT devices. His research has led to publications of more than 50 technical papers in international journals and conference proceedings, and filed two China patents.

Dr. Liang is an Associate Editor for *IET Circuits, Devices and Systems* and the General Chair of the 2nd International Conference on Vibration and Energy Harvesting Applications. He is a member in the Technical Committee of Power and Energy Circuits and Systems in IEEE Circuits and Systems Society, and the Energy Harvesting Technical Committee in Adaptive Structures and Material Systems Branch, ASME Aerospace Division. He has also served as a Program Committee Member in SPIE Smart Structures + Nondestructive Evaluation Conference. He is a recipient of the Best Student Contributions Award in the 19th International Conference on Adaptive Structures and Technologies, two Best Paper Awards in the IEEE International Conference on Information and Automation, the Postgraduate Research Output Award from The Chinese University of Hong Kong, and the Excellent Research Award 2018 from ShanghaiTech University.

Minfan Fu (Senior Member, IEEE) received the B.S., M.S., and Ph.D. degrees in electrical and computer engineering from the University of Michigan-Shanghai Jiao Tong University Joint Institute, Shanghai Jiao Tong University, Shanghai, China, in 2010, 2013, and 2016, respectively.

From 2016 to 2018, he held a Postdoctoral position with the Center for Power Electronics Systems, Virginia Polytechnic Institute and State University, Blacksburg, VA, USA. He is currently an Assistant Professor with the School of Information Science and Technology, ShanghaiTech University, Shanghai, China. His research interests include megahertz wireless power transfer, high-frequency power conversion, high-frequency magnetic design, and application of wide-bandgap devices. He holds one U.S. patent, three Chinese patents, and has authored or coauthored more than 50 papers in prestigious IEEE journals and conferences.

Dr. Fu is currently an Associate Editor for IEEE IES Industrial Electronics Technology News (ITeN) and serves as the Section Chair of several conference, such as IECON, IPEMC, VEH. His conference paper for IECON 2019 won the IES-SYPA Competition. He is the Tutorial Speaker for IPEMC 2020 and ISIE 2020.